

Received May 11, 2020, accepted May 28, 2020, date of publication June 9, 2020, date of current version June 24, 2020.

Digital Object Identifier 10.1109/ACCESS.2020.3001062

Spherical Wave Array Based Positioning for Vehicular Scenarios

MARCO ANTONIO MARQUES MARINHO^{1,2}, (Member, IEEE),
ALEXEY VINEL¹, (Senior Member, IEEE), FREDRIK TUFVESSON³, (Fellow, IEEE),
FELIX ANTREICH⁴, (Senior Member, IEEE),
JOÃO PAULO CARVALHO LUSTOSA DA COSTA², (Senior Member, IEEE),
AND EDISON PIGNATON DE FREITAS⁵, (Member, IEEE)

¹School of Information Technology, Halmstad University, 30118 Halmstad, Sweden

²Department of Electrical Engineering (ENE), University of Brasília (UnB), Brasília 70297-400, Brazil

³Department of Electrical and Information Technology, Lund University, 22100 Lund, Sweden

⁴Department of Telecommunications, Aeronautics Institute of Technology (ITA), São José dos Campos 12228-900, Brazil

⁵Informatics Institute, Federal University of Rio Grande do Sul (UFRGS), Porto Alegre 90040-060, Brazil

Corresponding author: Marco Antonio Marques Marinho (marco.marinho@hh.se)

This work was supported in part by the Knowledge Foundation through the framework of SafeSmart “Safety of Connected Intelligent Vehicles in Smart Cities” Synergy project (2019–2023), in part by the Swedish Foundation for Strategic Research (SSF) through the framework of Strategic Mobility Program (2019–2020), and in part by the ELLIIT Strategic Research Network.

ABSTRACT Smart vehicles are emerging as a possible solution for multiple concerns in road traffic, such as mobility and safety. This work presents radio localization methods based on simultaneous direction of arrival (DOA), time-delay, and range estimation using the SAGE algorithm. The proposed methods do not rely on external sources of information, such as global navigation satellite systems (GNSS). The proposed methods take advantage of signals of opportunity and do not require the transmission of location-specific signals; therefore, they do not increase the network load. A set of simulations using synthetic and measured data is provided to validate the proposed methods, and the results show that it is possible to achieve accuracy down to decimeter and centimeter-level.

INDEX TERMS Antenna arrays, localization, VANETs, vulnerable road user.

I. INTRODUCTION

Vehicular networks have been the focus of promising research in areas such as road safety, traffic control, automated vehicle control, and platooning [1]. Among these applications, road safety, automated vehicles, and road control require the vehicles to be able to process and to estimate the position of vulnerable road users (VRUs), as well as the position of the other vehicles in the vicinity, so that they can operate properly.

For the detection of VRUs, a variety of methods have been proposed [2]. These methods must be precise enough and have a low computational effort to meet different safety requirements regarding a multitude of possible situations. A set of requirements for VRU detection systems is presented in [3]. Most of these methods for VRU detection in the literature rely on computer vision [4]. These methods can provide an accuracy of up to 75% [5], [6], which might

The associate editor coordinating the review of this manuscript and approving it for publication was Wenming Cao¹.

be insufficient for safety-critical systems such as collision detection and prevention/avoidance.

The localization of other vehicles is also of interest and can be obtained by using a variety of methods. One such method is by using global navigation satellite systems (GNSS) for each vehicle to obtain an estimate of its location. GNSS such as the global positioning system (GPS) can provide location information with a mean error of 15 meters in urban environments [7]. However, the nominal accuracy of these systems is insufficient for emerging applications in intelligent transportation systems (ITS) such as platooning [8] or for safety-critical applications. Real-time kinematic (RTK) can be used to enhance GPS performance. However, this method is still susceptible to the presence of multipath and the occurrence of cycle slips, making its application challenging for real-time safety-critical systems [9]. Furthermore, GNSS requires that a set of at least four line-of-sight signals are received from different satellites, which is not always possible in dense urban environments. Thus, such shadowing of satellites leads to a possibly large number of outages in urban

environments. Other means of vehicle position estimation, such as received signal strength indicator (RSSI) [10] and dead reckoning [11] can also be used to assist GNSS positioning allowing its usage in safety-critical applications.

Approaches that leverage the presence of inertial sensors in smartphones inside a vehicle, using them to provide robust position estimates for vehicles in a network have been proposed [12], providing an accuracy of approximately 7 meters. Methods for localization in vehicular networks based on building a social model of the interactions of vehicles in the networks can provide position estimations with an accuracy of up to 10 meters [13]. While these methods provide an improvement over a GNSS only positioning solution, the accuracy provided is not sufficient for safety-critical applications in vehicular networks. Approaches that rely on a dedicated localization infrastructure can provide exact localization methods with an accuracy superior to one meter [14] at the cost of increased system complexity and may not be available outside of urban and busy roads.

Even in scenarios where the GNSS-based position provided by some vehicles can be assumed to be reliable and precise enough for an application at hand, problems such as spoofing and jamming can still emerge. In a spoofing attack, it is possible to falsify GNSS positioning information such that a vehicle will obtain a position estimate that has been altered by the attacker. Furthermore, since GNSS-based positioning information is usually spread using a data dissemination method [15], the position information can be falsified by the transmitting vehicle or by intermediary vehicles of the network. Position verification approaches [16] can mitigate, but not fully solve the problem of spoofing attacks.

Multiple-input multiple-output (MIMO) systems have been used in modern wireless communications standards to allow better spectral efficiency, faster data rates, and more robust communication. The usage of MIMO in vehicular network scenarios has been proposed to improve the network performance [17], suppress possible jamming attacks [18], and increase network capacity [19]. Here, we use multiple antennas at a vehicle for accurate position estimation of other vehicles and VRUs. It is well known that massive MIMO base station antennas having large apertures experience spherical wavefronts from close scatterers of users [20]. In this work, we use this property to aid the positioning.

Taking into account the problems and limitations of pure GNSS, RSSI, collaborative social based methods, and the versatility of MIMO-based systems, this work proposes an extension of the results presented in [21]. In [21], the usage of a variant of the space alternating generalized expectation maximization (SAGE) [22]–[24] algorithm for joint direction of arrival (DOA), time-delay, and range estimation to determine the position of VRUs or other vehicles was proposed. This work presents a novel joint parameter estimation, capable of improving the estimation accuracy. Furthermore, a method for obtaining an initial position estimation to initialize SAGE and avoiding convergence to local maxima is also presented; furthermore, the performance of the proposed

methods are tested with a real experimental setup. The proposed approach takes advantage of signals of opportunity transmitted by other vehicles or, for instance, by the cellphones of VRUs to estimate their relative positions. Since smartphone adoption in countries such as the U.S.A. is now higher than 90% [25], the signals transmitted by cellphones being carried by VRUs are excellent candidates for signals of opportunity for positioning. The proposed method allows that the position of a VRU is simultaneously estimated by all vehicles within its communication range. This approach does not require the transmission of localization specific messages and time synchronization between different nodes. Thus, it does not introduce extra network load in the mobile network. When compared to ultra wideband (UWB) radar systems, which can also be used to locate obstacles [26], the proposed method has the advantage of being able to detect VRUs that are not in direct line-of-sight as long as the transmitted signal is not fully obstructed.

The remainder of this work is divided into five sections. Section II details the data model assumed for this work while section IV details the proposed method. The performance of the proposed method is assessed in section VI. Finally, conclusions are drawn in section VII.

II. DATA MODEL

This work assumes that L wavefronts are received by a uniform linear array (ULA) composed of M antenna elements. The received signal uses an orthogonal frequency-division multiplexing (OFDM) scheme with of K subcarriers. The model considers a spherical wave front, taking into account the curvature of the propagating electromagnetic field [20]. Using the Fresnel approximation, after removing the cyclic prefix and taking the discrete Fourier transform (DFT) of the received signal the space-frequency response of the k th subcarrier received at antenna m at time snapshot t can be written as

$$y_{m,k}[t] = \sum_{l=1}^L s_k[t] \alpha_{k,l}[t] e^{j\omega_l(m-1) + \psi_l(m-1)^2} \cdot e^{j2\pi k \Delta_f \tau_l} + n_{m,k}[t], \quad (1)$$

where

$$\omega_l = -j \frac{2\pi \Delta_m \sin(\theta_l)}{\lambda}, \quad (2)$$

and

$$\psi_l = j \frac{\pi \Delta_m^2 \cos^2(\theta_l)}{\lambda r_l}, \quad (3)$$

where $s_k[t]$ is the symbol transmitted on the k th subcarrier at time instant t , $\alpha_{k,l}[t]$ is the complex channel gain coefficient of the l th wavefront and the k th subcarrier at snapshot t , Δ_m is the separation between antenna elements of the array, θ_l is the DOA of the l th wavefront, r_l is the range of the l th wavefront, λ is the wavelength of the carrier frequency, Δ_f is the frequency separation between the subcarriers of the OFDM signal, τ_l is the propagation delay (time-delay) of

the l th received signal, and $n_{m,k}[t]$ is additive complex white Gaussian noise.

The signal can be re-written in a matrix form as

$$\mathbf{Y}[t] = \mathbf{A}(\mathbf{S}^T[t] \circ \mathbf{Z}^T) + \mathbf{N}[t] \quad (4)$$

where \circ denotes the Hadamard-Schur product, the DOA and range steering matrix and the time-delay steering matrix can be given as

$$\mathbf{A} = [\mathbf{a}(\theta_1, r_1), \mathbf{a}(\theta_2, r_2), \dots, \mathbf{a}(\theta_L, r_L)] \in \mathbb{C}^{M \times L}, \quad (5)$$

$$\mathbf{Z} = [\mathbf{z}(\tau_1), \mathbf{z}(\tau_2), \dots, \mathbf{z}(\tau_L)] \in \mathbb{C}^{K \times L}, \quad (6)$$

with

$$\mathbf{a}(\theta_l, r_l) = [1, e^{j\omega_l + \psi_l}, \dots, e^{j\omega_l(M-1) + \psi_l(M-1)^2}]^T \in \mathbb{C}^{M \times 1}, \quad (7)$$

$$\mathbf{z}(\tau_l) = [e^{j2\pi \Delta_f \tau_l}, \dots, e^{j2\pi K \Delta_f \tau_l}]^T \in \mathbb{C}^{K \times 1}, \quad (8)$$

where

$$\mathbf{S}[t] = [\boldsymbol{\alpha}_1[t] \circ \mathbf{s}[t], \boldsymbol{\alpha}_2[t] \circ \mathbf{s}[t], \dots, \boldsymbol{\alpha}_L[t] \circ \mathbf{s}[t]] \in \mathbb{C}^{K \times L}, \quad (9)$$

with symbol vector

$$\mathbf{s}[t] = [s_1[t], s_2[t], \dots, s_K[t]]^T \in \mathbb{C}^{K \times 1}, \quad (10)$$

and the vector of complex channel gains of the l th wavefront is given as

$$\boldsymbol{\alpha}_l = [\alpha_{1,l}[t], \alpha_{2,l}[t], \dots, \alpha_{K,l}[t]]^T \in \mathbb{C}^{K \times 1}. \quad (11)$$

Rearranging using the vec-operator we can write^{1 2}

$$\begin{aligned} \text{vec}\{\mathbf{Y}[t]\} &= \text{vec}\{\mathbf{A}(\mathbf{S}^T[t] \circ \mathbf{Z}^T)\} + \text{vec}\{\mathbf{N}[t]\} \\ &= (\mathbf{I}_K \otimes \mathbf{A})\text{vec}\{\mathbf{S}^T[t] \circ \mathbf{Z}^T\} + \text{vec}\{\mathbf{N}[t]\} \\ &= (\mathbf{I}_K \otimes \mathbf{A}) \underbrace{\text{diag}\{\text{vec}\{\mathbf{Z}^T\}\}}_{=\tilde{\mathbf{Z}}} \underbrace{\text{vec}\{\mathbf{S}^T[t]\}}_{=\tilde{\mathbf{s}}[t]} \\ &\quad + \underbrace{\text{vec}\{\mathbf{N}[t]\}}_{=\tilde{\mathbf{n}}[t]} \\ &= (\mathbf{I}_K \otimes \mathbf{A}) \tilde{\mathbf{Z}} \tilde{\mathbf{s}}[t] + \tilde{\mathbf{n}}[t], \end{aligned} \quad (12)$$

where \otimes denotes the Kronecker product. Collecting several snapshots with $t = 1, \dots, T$ we can write

$$\tilde{\mathbf{Y}} = (\mathbf{I}_K \otimes \mathbf{A}) \tilde{\mathbf{Z}} \tilde{\mathbf{S}} + \tilde{\mathbf{N}} \in \mathbb{C}^{MK \times T} \quad (13)$$

with

$$\tilde{\mathbf{S}} = [\tilde{\mathbf{s}}[1], \tilde{\mathbf{s}}[2], \dots, \tilde{\mathbf{s}}[T]] \quad (14)$$

and

$$\mathbb{E}[\text{vec}\{\tilde{\mathbf{N}}\}\text{vec}\{\tilde{\mathbf{N}}\}^H] = \sigma_n^2 \mathbf{I}_{MKT}. \quad (15)$$

¹For $\mathbf{A} \in \mathbb{C}^{M \times N}$, $\mathbf{B} \in \mathbb{C}^{N \times P}$, and $\mathbf{C} \in \mathbb{C}^{P \times Q}$, $\text{vec}\{\mathbf{ABC}\} = (\mathbf{C}^T \otimes \mathbf{A})\text{vec}\{\mathbf{B}\}$

²For $\mathbf{D} \in \mathbb{C}^{M \times N}$ and $\mathbf{E} \in \mathbb{C}^{M \times N}$, $\text{vec}\{\mathbf{D} \circ \mathbf{E}\} = \text{vec}\{\mathbf{D}\} \circ \text{vec}\{\mathbf{E}\} = \text{diag}\{\text{vec}\{\mathbf{D}\}\}\text{vec}\{\mathbf{E}\}$

III. SPACE-ALTERNATING GENERALIZED EXPECTATION MAXIMIZATION (SAGE) ALGORITHM

The SAGE algorithm [22] is a generalization of the well known expectation maximization (EM) algorithm [27]. Both algorithms are used to derive maximum likelihood estimates in an iterative fashion. SAGE and EM utilize the concept of a hidden data space to avoid dealing with the complete observable data space. In the case of a signal received at the array, the complete data can be written as a function of the hidden data space

$$\tilde{\mathbf{Y}} = \mathbf{X}_1 + \mathbf{X}_2 + \dots + \mathbf{X}_L \quad (16)$$

where the hidden data space (one noisy wavefront) can be given as

$$\begin{aligned} \mathbf{X}_l &= (\mathbf{I}_K \otimes \mathbf{a}(\theta_l, r_l))\text{diag}\{\mathbf{z}(\tau_l)\}\tilde{\mathbf{S}}_l + \tilde{\mathbf{N}}_l \\ &= \mathbf{H}(\mathbf{p}_l)\tilde{\mathbf{S}}_l + \tilde{\mathbf{N}}_l. \end{aligned} \quad (17)$$

with

$$\tilde{\mathbf{S}}_l = [\boldsymbol{\alpha}_l[1] \circ \mathbf{s}[1], \boldsymbol{\alpha}_l[2] \circ \mathbf{s}[2], \dots, \boldsymbol{\alpha}_l[T] \circ \mathbf{s}[T]] \in \mathbb{C}^{K \times T} \quad (18)$$

and

$$\mathbf{p}_l = [\theta_l, r_l, \tau_l]^T. \quad (19)$$

The noise terms $\tilde{\mathbf{N}}_l$ are statistically independent with variance $\beta_l \sigma_n^2$.

The SAGE algorithm performs two different steps, the expectation and the maximization steps. The expectation step can be given as

$$\begin{aligned} \hat{\mathbf{X}}_l &= \mathbb{E}_{\mathbf{X}_l} [\mathbf{X}_l | \tilde{\mathbf{Y}}; \hat{\mathbf{p}}] \\ &= (1 - \beta_l) \mathbf{H}(\hat{\mathbf{p}}_l) \hat{\mathbf{S}}_l \\ &\quad + \beta_l \left(\tilde{\mathbf{Y}} - \sum_{\substack{l'=1 \\ l' \neq l}}^L \mathbf{H}(\hat{\mathbf{p}}_{l'}) \hat{\mathbf{S}}_{l'} \right) \end{aligned} \quad (20)$$

where the parameter vector is

$$\mathbf{p} = [\boldsymbol{\theta}^T, \mathbf{r}^T, \boldsymbol{\tau}^T]^T \quad (21)$$

with $\boldsymbol{\theta} = [\theta_1, \dots, \theta_L]^T$, $\mathbf{r} = [r_1, \dots, r_L]^T$, $\boldsymbol{\tau} = [\tau_1, \dots, \tau_L]^T$, and we assume that an estimate of $\tilde{\mathbf{S}}$ denoted by $\hat{\tilde{\mathbf{S}}}$ is available. Choosing $\beta_l = 1$ for each wavefront the convergence rate of the SAGE algorithm is largest due to the amount of new information introduced to the estimate of the hidden data space \mathbf{X}_l [23]. Thus, the expectation step can be given as

$$\hat{\mathbf{X}}_l = \tilde{\mathbf{Y}} - \sum_{\substack{l'=1 \\ l' \neq l}}^L \mathbf{H}(\hat{\mathbf{p}}_{l'}) \hat{\mathbf{S}}_{l'}. \quad (22)$$

The maximization step derives new (updated) estimates of the parameters of all wavefronts. Assuming that \mathbf{X}_l are independent, that $\tilde{\mathbf{Y}}$ and \mathbf{X}_l are realizations of multivariate Gaussian random variables, and with $\hat{\mathbf{X}}_l$ at hand from the expectation

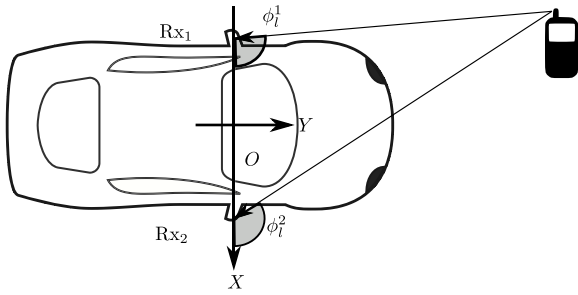


FIGURE 1. Vehicle equipped with antenna arrays at the wing mirrors.

step, we can maximize the log-likelihood of the hidden data space solving

$$\begin{aligned} \hat{\mathbf{p}}_l &= \arg \max_{\mathbf{p}_l} \left\{ 2 \operatorname{Re} \left\{ \operatorname{vec} \{ \mathbf{H}(\mathbf{p}_l) \hat{\mathbf{S}}_l \}^H \operatorname{vec} \{ \hat{\mathbf{X}}_l \} \right\} \right. \\ &\quad \left. - \{ \| \mathbf{H}(\mathbf{p}_l) \hat{\mathbf{S}}_l \|_F^2 \} \right\} \\ &= \arg \max_{\mathbf{p}_l} \left\{ J(\mathbf{p}_l, \hat{\mathbf{X}}_l, \hat{\mathbf{S}}_l) \right\}, \end{aligned} \quad (23)$$

where $\| \cdot \|_F^2$ denotes the Frobenius norm.

This problem can even be broken down to one-dimensional problems which are solved sequentially for each parameter of \mathbf{p}_l .

The SAGE algorithm performs the expectation and the maximization step iteratively, wavefront-by-wavefront until the parameter estimates converge.

IV. SCENARIO DESCRIPTION

This work assumes that the vehicles connected to the VANET are equipped with two linear antenna arrays (subarrays) at two distinct locations on their frames. Figure 1 presents an example of a vehicle with antenna arrays equipped at the wing mirror position estimating the position of a VRU. Alternatively, these arrays can be placed, for instance, at opposing ends of the windshield or by the headlights.

V. ARRAY PROCESSING ALGORITHMS FOR LOCALIZATION

This section presents three methods for estimating the position of a transmitter in a vehicular network context, namely the flip-flop, joint, and DOA only methods.

A. FLIP-FLOP ESTIMATION

The flip-flop method is an iterative approach that consists of individual parameter estimation at each subarray. The estimates obtained at each subarray are then used to update the estimates at the remaining one.

Following the data model presented in (13), the expectation step of the SAGE algorithm is given by

$$\hat{\mathbf{X}}_l^q = \tilde{\mathbf{Y}}^q - \sum_{\substack{l'=1 \\ l' \neq l}}^L \left(\mathbf{H}(\hat{\mathbf{p}}_{l'}^q) \hat{\mathbf{S}}_{l'} \right), \quad (24)$$

where $\tilde{\mathbf{Y}}^q \in \mathbb{C}^{MK \times T}$ is the received data of the q th subarray, with $q \in [1, 2]$, following the signal model given in (13),

$\hat{\mathbf{X}}_l^q$ is the estimate for the signal received from the l th source at the q th subarray and

$$\mathbf{p}_l^q = \left[\hat{\theta}_l^q, \hat{r}_l^q, \hat{\tau}_l^q \right]^T, \quad (25)$$

where $\hat{\theta}_l^q$, $\hat{\tau}_l^q$, and \hat{r}_l^q are the azimuth, time-delay, and range estimates for the l th source at the q th subarray, respectively.

In the maximization step three one-dimensional optimization problems are solved which can be given as

$$\hat{\theta}_l^q = \arg \max_{\theta_l^q} \left\{ J \left(\mathbf{p}_l^q, \hat{\mathbf{X}}_l^q, \hat{\mathbf{S}}_l \right) \right\}, \quad (26)$$

$$\hat{r}_l^q = \arg \max_{r_l^q} \left\{ J \left(\mathbf{p}_l^q, \hat{\mathbf{X}}_l^q, \hat{\mathbf{S}}_l \right) \right\}, \quad (27)$$

$$\hat{\tau}_l^q = \arg \max_{\tau_l^q} \left\{ J \left(\mathbf{p}_l^q, \hat{\mathbf{X}}_l^q, \hat{\mathbf{S}}_l \right) \right\}. \quad (28)$$

This process is iteratively performed until the estimate for all parameters has converged.

Once range and DOA have been estimated at one of the subarrays, an estimate of the position of the transmitter can be obtained. Assuming that the center of a line crossing the car and both wing mirrors to be the origin of the reference coordinate system, denoted as O . It is necessary to obtain the angle ϕ_l^q , which, as shown in Figure 1, is a complementary angle to θ_l^q . Thus, the relationship between ϕ_l^q and θ_l^q is given by

$$\phi_l^q = \begin{cases} -(\frac{\pi}{2} + \hat{\theta}_l^q), & \hat{\theta}_l^q < 0 \\ (\frac{\pi}{2} - \hat{\theta}_l^q), & \hat{\theta}_l^q \geq 0. \end{cases} \quad (29)$$

With an estimate of this parameter at hand and considering the coordinate system shown in Figure 1, an estimate of the position of the l th transmitter with respect to the signal received at the q th subarray Rx_q is given by

$$x_l^q = \hat{r}_l^q \cos(\phi_l^q) + x_{Rx_q} \quad (30)$$

and

$$y_l^q = \hat{r}_l^q \sin(\phi_l^q), \quad (31)$$

where x_l^q and y_l^q are the estimates for the coordinates of the l th transmitter and x_{Rx_q} is the position of the center of the q th subarray on the X axis as illustrated in Figure 1. A position estimated concerning one of the subarrays then can be mapped into a DOA and range estimation at the other subarray. Thus, once the full set of the parameters from one of the subarrays has been estimated after a SAGE iteration, the position estimate extracted from such parameters can be used to update the current estimates for the remaining subarray before its next SAGE iteration. The switching between subarrays improves the convergence rate of the SAGE algorithms and prevents the search from running into a local maximum and thus converging to an imprecise estimate. Figure 2 presents a block diagram illustrating the flow of the proposed method.

Under ideal conditions, after the SAGE algorithm has converged for both subarrays, the transmitter position estimate

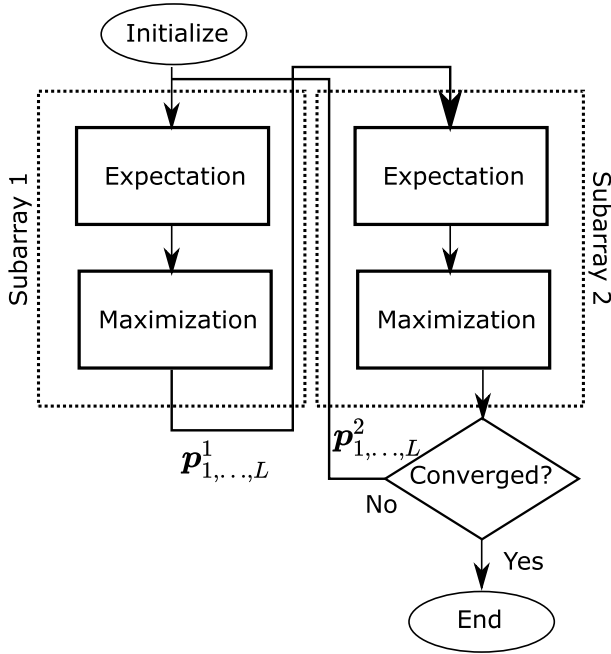


FIGURE 2. Block diagram for the proposed flip-flip method.

would be identical for both subarrays, that is, $\hat{x}_l^1 = \hat{x}_l^2$ and $\hat{y}_l^1 = \hat{y}_l^2$. However, due to the noise, numerical errors and further imprecision introduced during the estimation, they will be different, i.e., $\hat{x}_l^1 \neq \hat{x}_l^2$ and $\hat{y}_l^1 \neq \hat{y}_l^2$. To solve this, the final estimate can be given as a function of the estimates for each of the subarrays as

$$\hat{x}_l = \frac{\gamma \hat{x}_l^1 + \nu \hat{x}_l^2}{\gamma + \nu} \quad (32)$$

and

$$\hat{y}_l = \frac{\gamma \hat{y}_l^1 + \nu \hat{y}_l^2}{\gamma + \nu}, \quad (33)$$

where γ and ν are weighting coefficients that represent how reliable are the position estimates at each subarray. These coefficients can be set, for instance, as a function of the received signal power at each subarray. In this case γ and ν are given by

$$\gamma = \frac{\left(\mathbf{z}(\hat{\tau}_l^1) \otimes \mathbf{a}(\hat{\theta}_l^1, \hat{r}_l^1) \right)^H \mathbf{Y}^1 \mathbf{Y}^{1H} \left(\mathbf{z}(\hat{\tau}_l^1) \otimes \mathbf{a}(\hat{\theta}_l^1, \hat{r}_l^1) \right)}{\left(\mathbf{z}(\hat{\tau}_l^1) \otimes \mathbf{a}(\hat{\theta}_l^1, \hat{r}_l^1) \right)^H \left(\mathbf{z}(\hat{\tau}_l^1) \otimes \mathbf{a}(\hat{\theta}_l^1, \hat{r}_l^1) \right) \text{tr} \left(\mathbf{Y}^1 H \mathbf{Y}^1 \right)}, \quad (34)$$

and

$$\nu = \frac{\left(\mathbf{z}(\hat{\tau}_l^2) \otimes \mathbf{a}(\hat{\theta}_l^2, \hat{r}_l^2) \right)^H \tilde{\mathbf{Y}}^2 \tilde{\mathbf{Y}}^{2H} \left(\mathbf{z}(\hat{\tau}_l^2) \otimes \mathbf{a}(\hat{\theta}_l^2, \hat{r}_l^2) \right)}{\left(\mathbf{z}(\hat{\tau}_l^2) \otimes \mathbf{a}(\hat{\theta}_l^2, \hat{r}_l^2) \right)^H \left(\mathbf{z}(\hat{\tau}_l^2) \otimes \mathbf{a}(\hat{\theta}_l^2, \hat{r}_l^2) \right) \text{tr} \left(\mathbf{Y}^2 H \mathbf{Y}^2 \right)}. \quad (35)$$

The line-of-sight (LOS) signal can then be selected by finding the received signal with the smallest propagation

delay

$$\hat{\tau}_{\text{LOS}} = \min[\hat{\tau}_1, \hat{\tau}_2, \dots, \hat{\tau}_L] \quad (36)$$

B. JOINT DIRECT POSITION ESTIMATION

To avoid performing two independent estimations, one at each subarray, and consequently having to merge both estimates, the estimation problem can be rewritten using a different parameterization. A set of coordinates for a transmitter will have a unique mapping to a given set of DOA and range at each subarray. Thus, the problem can be directly written concerning these parameters common to both subarrays, i.e., the coordinates of a transmitter in the coordinate system shown in Figure 1. The range given in (1) can be written as

$$r_l^q = \sqrt{(x_{Rx_q} - x_l)^2 + (y_l)^2}, \quad (37)$$

the DOA θ_l^q can be given as

$$\theta_l^q = \arctan \left(\frac{y_l}{x_{Rx_q} - x_l} \right), \quad (38)$$

and

$$\tau_l^q = \frac{\sqrt{(x_{Rx_q} - x_l)^2 + (y_l)^2}}{c}, \quad (39)$$

where $x_l = x_l^1 = x_l^2$, $y_l = y_l^1 = y_l^2$, and c is the speed of light.

Note, that after the re-parameterization, x_l and y_l are the only unknowns, and are common to both subarrays. Thus, to jointly estimate these parameters an augmented received signal matrix containing the inputs of both subarrays Rx_1 and Rx_2 can be defined as

$$\tilde{\mathbf{Y}} = \begin{bmatrix} \tilde{\mathbf{Y}}^1 \\ \tilde{\mathbf{Y}}^2 \end{bmatrix} \in \mathbb{C}^{2MK \times T}. \quad (40)$$

SAGE can then be applied to the data $\tilde{\mathbf{Y}}$. The hidden data space can be defined as

$$\tilde{\mathbf{Y}} = \tilde{\mathbf{X}}_1 + \tilde{\mathbf{X}}_2 + \dots + \tilde{\mathbf{X}}_L, \quad (41)$$

where

$$\tilde{\mathbf{X}}_l = \tilde{\mathbf{H}}(\bar{\mathbf{p}}_l) \tilde{\mathbf{S}}_l + \tilde{\mathbf{N}}_l, \quad (42)$$

with

$$\tilde{\mathbf{H}}(\bar{\mathbf{p}}_l) = \begin{bmatrix} \mathbf{H}(\mathbf{p}_l^1) \\ \mathbf{H}(\mathbf{p}_l^2) \end{bmatrix} \in \mathbb{C}^{2MK \times 1}, \quad (43)$$

and

$$\tilde{\mathbf{S}}_l = \begin{bmatrix} \tilde{\mathbf{S}}_l^1 \\ \tilde{\mathbf{S}}_l^2 \end{bmatrix} \in \mathbb{C}^{2K \times T}, \quad (44)$$

where $\tilde{\mathbf{S}}_l^1$ and $\tilde{\mathbf{S}}_l^2$ include the symbols and channel gains received by each subarray. Here, $\bar{\mathbf{p}}_l$ is a unique parameter vector for both subarrays given by

$$\bar{\mathbf{p}}_l = [x_l, y_l]. \quad (45)$$

The expectation step for this parameterization is given by

$$\hat{\mathbf{X}}_l = \bar{\mathbf{Y}} - \sum_{\substack{l'=1 \\ l' \neq l}}^L \left(\hat{\mathbf{H}}(\bar{\mathbf{p}}_{l'}) \hat{\mathbf{S}}_{l'} \right). \quad (46)$$

Following (23), the optimization problem can be solved directly for the transmitter coordinates x_l and y_l and the maximization step can be given as

$$\hat{x}_l = \arg \max_{x_l} \left\{ J \left(\bar{\mathbf{p}}_l, \hat{\mathbf{X}}_l, \hat{\mathbf{S}}_l \right) \right\}, \quad (47)$$

$$\hat{y}_l = \arg \max_{y_l} \left\{ J \left(\bar{\mathbf{p}}_l, \hat{\mathbf{X}}_l, \hat{\mathbf{S}}_l \right) \right\}. \quad (48)$$

Since the data received by the subarrays is jointly used to perform the estimation, the distance between both subarrays contributes to the accuracy of the estimates obtained, as it improves the identifiability of the range parameter.

The method is, however, not without its drawbacks. The computational load, when employing the proposed joint estimation, is higher than the computational load involved in the flip-flop method. The search space for the flip-flop method is limited to $[-\frac{\pi}{2}, \frac{\pi}{2}]$ in the DOA estimation, and to $[0, r_{max}]$ in the range estimation, where r_{max} is the maximum assumed communication distance. For the joint estimation method, the search space, in theory, is $[0, r_{max}]$ for both x_l and y_l , assuming that a transmitter can be located anywhere within a semicircle with radius r_{max} . While the search space may be reduced by assuming certain constraints on a transmitting vehicle, it might lead to large biases in the presence of non-line-of-sight (NLOS) components that are not arriving from a position contained within this reduced search space. Due to the restricted search space, such components will not be properly estimated, and, therefore, their contribution to the received signal will not be properly separated from the remaining components, hence leading to estimation biases.

C. DOA ONLY ESTIMATION

Alternatively, a planar wavefront model can be assumed. In this case, a position estimate can be obtained by performing individual parameter estimations at each subarray independently. Using the DOA estimates at each subarray and considering the coordinate system shown in Figure 1 the lines representing the signals received at Rx_1 and Rx_2 can be given as

$$y_l^1 = \tan(\phi_l^1)x_l^1 - \tan(\phi_l^1)x_{Rx_1}, \quad (49)$$

$$y_l^2 = \tan(\phi_l^2)x_l^2 - \tan(\phi_l^2)x_{Rx_2}. \quad (50)$$

The position of the transmitter array can be obtained by calculating the point where (49) and (50) intersect, which can be accomplished by solving

$$x_l = \frac{\tan(\phi_l^1)x_{Rx_1} - \tan(\phi_l^2)x_{Rx_2}}{\tan(\phi_l^1) - \tan(\phi_l^2)}, \quad (51)$$

$$y_l = \frac{\tan(\phi_l^1)\tan(\phi_l^2)(x_{Rx_2} - x_{Rx_1})}{\tan(\phi_l^2) - \tan(\phi_l^1)}. \quad (52)$$

Here, the selection of which received signal component represents the LOS signal can be made by selecting the signal with the largest power.

While this method requires only DOA estimates at each of the subarrays, the derived position estimates are highly sensitive to errors in the DOA estimates as they are a nonlinear function of these DOA estimates.

D. APPLICABILITY OF TIME-DELAY ESTIMATION FOR POSITIONING

Another possible solution for estimating the transmitter's position is to use time-delays that have been estimated. Using the estimates of the delays $\hat{\tau}_l^q$, an estimation of the range between the transmitting and receiving array can be obtained as

$$\hat{r}_l^q = c\hat{\tau}_l^q. \quad (53)$$

However, estimating the range using the time-delay is less robust than the one obtained through the SAGE estimation using the spherical wave model. That is because the time-delay can only be estimated concerning an internal reference at the receiver. That is, the time-delay estimation will be influenced by the synchronization between the transmitter and the receiver. Whatever error is present in synchronization will be present in the time-delay estimation, as the internal reference of the receiver will differ from the one of the transmitters. Therefore, unless a very reliable source of synchronization is present, this method of positioning is not suitable for safety-critical applications, as an error in time-delay estimation of just one nanosecond will already result in a ranging error of approximately 30 cm. If the synchronization between receiver and transmitter is to be relied on, the position of the transmitter can be estimated following (30) and (31) and substituting the range estimate for the one given in (53).

Another possible use for $\hat{\tau}_l^q$ is to aid in the selection of the LOS component. Assuming there is a LOS component, even if it is obstructed, its $\hat{\tau}_l^q$ estimate should be the smallest one, as reflected signals need to travel for longer to arrive at the receiver.

VI. SIMULATION RESULTS

This section presents a performance assessment of the proposed flip-flop and joint positioning methods. Subsection VI-A presents the results obtained for synthetic data, while subsection VI-B presents the results obtained using measured data.

A. RESULTS FOR SYNTHETIC DATA

In this section, the performance of the flip-flop and joint positioning algorithm is assessed by a set of numerical simulations. The simulation assumes two antenna subarrays at the rear-view mirrors; these are considered to be ULAs composed of $M = 5$ antennas with an inter-element spacing of $\Delta_m = \frac{\lambda}{2}$. For the simulations, this work assumes the transmitter is using the LTE standard, with the maximum fast Fourier transform size of 2048, of which 1200 are effective subcarriers and

$\Delta_f = 15$ kHz subcarrier spacing. We assume that $T = 100$ OFDM symbols have been measured with a normal cyclic prefix. Channel estimation and symbol decision are made by selection the received data at one antenna of each subarray and following the standard LTE decoding block. Frequency correlation is introduced following the method proposed in [28]. A bandwidth ranging from a single tonal signal (narrowband) to 20 MHz (standard LTE channel bandwidth) is considered to assess the performance of the proposed methods concerning the bandwidth of the transmitted signal. The ranging estimation is done only using the range parameter present in the spherical wave model. The antenna arrays are assumed to be placed 1.80 m apart from each other, an average car width. For the sake of completeness and unless stated otherwise, the simulations assume the presence of 3 NLOS multipath components with respective scatterers randomly located between the transmitter and the receiving array. The number of components L that are received is unknown. The model order L is estimated in the initialization of the SAGE algorithm. Unless stated otherwise, the Rician K factor for the simulations is kept fixed at 3 dB. The SAGE algorithm for both the flip-flop and joint estimation methods is initialized using position estimates obtained using the DOA only method. The root mean squared error (RMSE) is derived based on 1000 Monte Carlo runs and is calculated as

$$RMSE = \sqrt{\frac{1}{I} \sum_{i=1}^I \left((\hat{x}_l^{(i)} - x)^2 + (\hat{y}_l^{(i)} - y)^2 \right)}, \quad (54)$$

where $\hat{x}_l^{(i)}$ and $\hat{y}_l^{(i)}$ the estimates of the i th Monte Carlo run and x and y denote the true location of the transmitter.

Figure 3 presents an assessment of the performance of the proposed methods under varying signal-to-noise ratio (SNR). The distance between the receiving array and the transmitter is kept fixed at 20 m, and the SNR varies from -5 to 25 dB. For the joint estimation method, the extra frequency samples provided by a broader bandwidth have a large impact on performance. In the narrowband case, SAGE does not converge to an accurate estimate under low to moderate SNR conditions. However, even under the assumption of a narrowband signal, sub-meter accuracy is achievable at moderate SNRs. With larger bandwidths, the joint estimation method is capable of sub-centimeter accuracy, even for low SNRs. The flip-flop method's performance is shown to be more stable in the narrowband case. However, it is still outperformed by the joint method for high SNRs.

The second set of simulations studies the performance of the proposed methods dependent on the distance to the transmitter. The SNR is kept fixed at 15 dB, and the distance between the receiving array and the transmitter varies from 5 to 50 meters. The results shown in Figure 4 highlight that, for both methods, the accuracy is degraded as the distance to the transmitter increases. Despite having the worst performance, the flip-flop method is still capable of sub-meter performance for a transmitter up to a distance of 35 m in

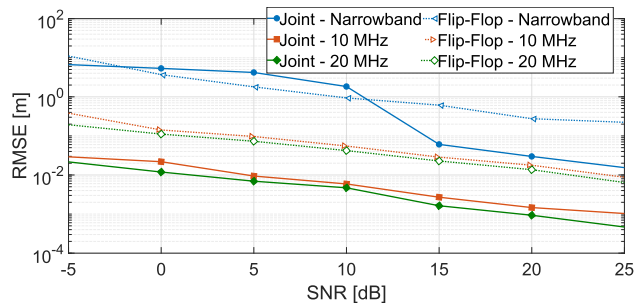


FIGURE 3. Position estimation error vs SNR.

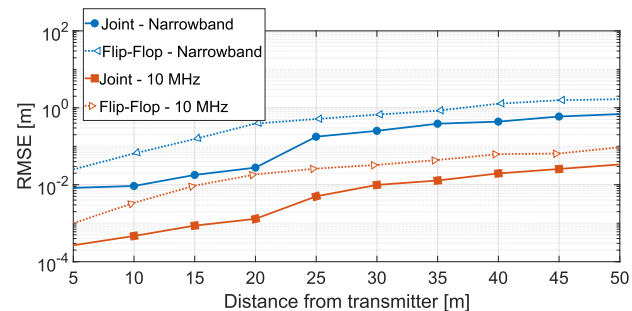


FIGURE 4. Position estimation error vs distance from source.

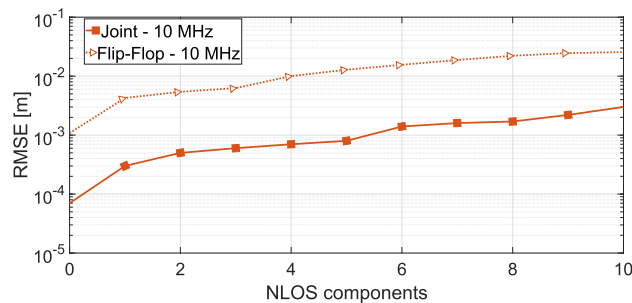


FIGURE 5. Position estimation error vs number of NLOS components.

the narrowband case and, in the broadband case, decimeter performance up to a distance of 50 m.

Figure 5 presents the performance of the proposed algorithms with respect to the number of multipath components (MPCs) with K-factor fixed at 3 dB. The SNR is kept fixed at 15 dB, and the distance from the transmitter to the receiver is fixed at 20 m. The results show that the number of MPCs has only a moderate impact on the performance of the proposed method. As the number of MPCs increases, the probability of closely spaced sources increases, and the probability of MPCs with similar DOAs and time-delays increases, leading to a possible higher spatial and frequency correlation. The increased spatial correlation is especially harmful as it can make an MPC non-separable from the LOS component by SAGE. In the unlikely scenario where only the LOS component is present, the performance of the proposed methods is significantly improved.

Figure 6 assesses the effect of the K-factor on the proposed methods, the number of MPCs is kept fixed at six, and the K-factor is varied.

Figure 7 shows the estimation error of x_l and y_l of the position estimation. For this set of simulations, the distance

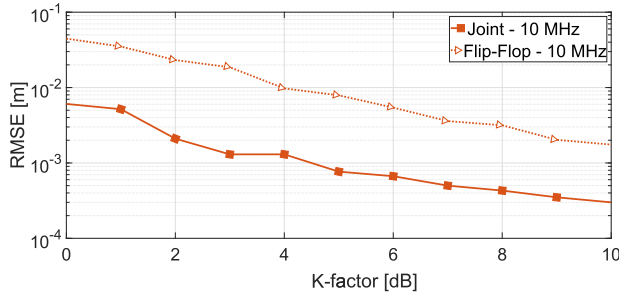


FIGURE 6. Position estimation error vs K-factor.

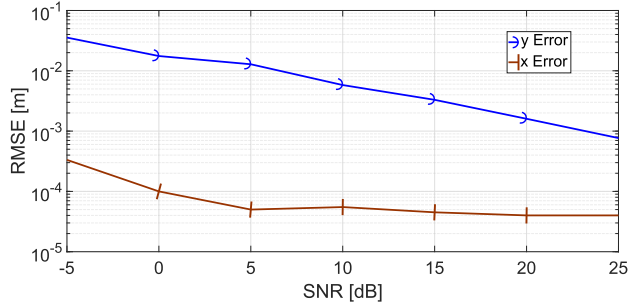


FIGURE 7. Position estimation error over the x- and y-axes.

from the transmitter is fixed at 20 m, the performance presented is for the joint estimation method using a 10 MHz bandwidth. The results highlight that most of the estimation error is a result of the estimation errors of y_l . The ranges r_l are present only in ψ_l of the model given in (3). This component has a nonlinear relationship with the range parameter. Thus, even small errors in the identification and estimation of this component will lead to somewhat significant errors in the range estimate. However, even for low SNRs, the error of y_l is kept below one centimeter.

B. RESULTS FOR REAL DATA

As a proof of concept and to assess the performance of the proposed method in a real-world scenario, a measured data set is used. The measurements were performed using a center frequency of 2.6 GHz with 50 MHz of bandwidth. The antenna array is a ULA composed of 128 elements with inner element spacing of $\frac{\lambda}{2} = 5.8$ cm and spanning 8 meters. Out of the data set, we select two subsets of $M = 5$ antennas separated by approximately 1.8 m and use 10 MHz out of the 50 MHz available bandwidth in the measurements. The measurements were performed at the E-building of the Faculty of Engineering LTH, Lund University, Sweden. The antenna array was placed on the roof of the building, and the users were located on a patio overlooked by the array. Figure 8 presents a picture of the antenna array that was used for the measurements. As seen, the scenario for the measurements is not vehicular, but it serves as a proof of concept and contains many scatterers besides users as would be expected in an urban vehicular scenario. Figure 9 presents a map of the location of users on the patio considered for the measurements.

The positions of users 10, 15, 19, and 26 are chosen to be estimated, as depicted in Figure 9, to assess the performance



FIGURE 8. Antenna array used for measurements.

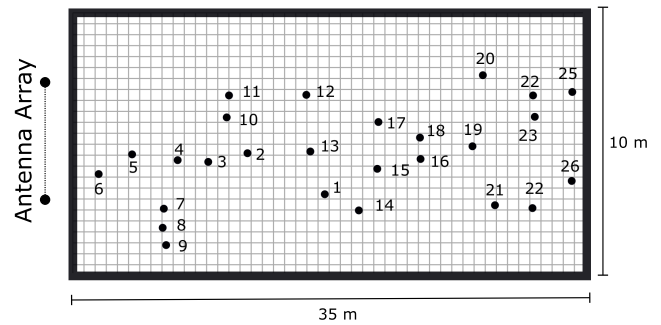


FIGURE 9. User distribution for measurements.

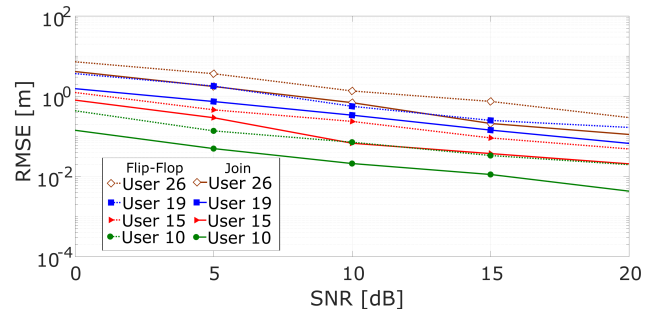


FIGURE 10. Position estimation error for measured data.

of the proposed algorithms using real data. One of the shortcomings of the measured data set is that the elevation of the antenna array is not the horizon, as assumed in the model of this work, which might introduce some bias on the final position estimates.

Figure 10 presents the performance of the proposed position estimation methods when applied to the measured data set. Synthetic noise is added to the measurements to assess the performance of the proposed method concerning SNR in real scenarios. The performance behaves similarly to the results obtained with the simulated data set, users that are located further away from the array will have a smaller localization accuracy than those closer to the array.

The overall difference in performance from the real data set to the simulated data set is most likely due to noise already

present in the measurements, which is introduced by instruments such as power amplifiers and converters used in the set-up. Despite these imprecisions, the proposed joint estimation method was capable of achieving sub-meter performance for an added SNR of up to 10 dB for all selected users and presented centimeter-level accuracy for an SNR of 20 dB. The flip-flop method was also able to achieve sub-meter accuracy for SNRs larger than 10 dB with a faster convergence rate when compared to the joint estimation method.

VII. CONCLUSION

This work presented novel methods for position estimation for vehicular network systems. The proposed methods rely on using a spherical wave model and employing the SAGE algorithm to provide position estimates. The presented flip-flop method estimates the DOA and range of the received signals and the respective transmitter at two subarrays separately and uses the results of one array to update the problem on the remaining one. This method has a fast convergence time but has limited accuracy.

The proposed joint estimation method is used to obtain a direct estimate of the coordinates of the transmitter by parameterizing the problem directly with respect to such coordinates. While this method has a slower convergence time, it is capable of providing superior performance compared to the flip-flop method.

This work shows that the proposed methods are capable of achieving centimeter-level accuracy for moderate distances and large SNRs, and provide sub-meter accuracy for moderate SNRs, using a real data set obtained from measurements.

The proposed methods can be used as a stand-alone localization estimation method for both vehicles and VRUs. Furthermore, they may be used for spoofing detection and mitigation, as they rely solely on estimating parameters from the physical layer. Such parameters are extremely hard to fake with hardware available today. The proposed methods do not require any specific data to be exchanged between the transmitter and the receiver and can be applied when any data exchange is happening on the network. Therefore, the proposed methods do not imply an increased network load.

ACKNOWLEDGMENT

The authors would like to thank Dr. Sohail Payami for his contributions to the measurements.

REFERENCES

- [1] V. Kumar, S. Mishra, and N. Chand, "Applications of VANETs: Present & future," *Commun. Netw.*, vol. 5, no. 1, p. 12, 2013.
- [2] T. Gandhi and M. M. Trivedi, "Pedestrian protection systems: Issues, survey, and challenges," *IEEE Trans. Intell. Transport. Syst.*, vol. 8, no. 3, pp. 413–430, Sep. 2007.
- [3] A. Habibovic and J. Davidsson, "Requirements of a system to reduce car-to-vulnerable road user crashes in urban intersections," *Accident Anal. Prevention*, vol. 43, no. 4, pp. 1570–1580, Jul. 2011.
- [4] D. M. Gavrilu, J. Giebel, and S. Munder, "Vision-based pedestrian detection: The protector system," in *Proc. IEEE Intell. Vehicles Symp.*, Jun. 2004, pp. 13–18.
- [5] P. Dollar, C. Wojek, B. Schiele, and P. Perona, "Pedestrian detection: An evaluation of the state of the art," *IEEE Trans. Pattern Anal. Mach. Intell.*, vol. 34, no. 4, pp. 743–761, Apr. 2012.
- [6] D. Gerónimo, A. M. López, A. D. Sappa, and T. Graf, "Survey of pedestrian detection for advanced driver assistance systems," *IEEE Trans. Pattern Anal. Mach. Intell.*, vol. 32, no. 7, pp. 1239–1258, Jul. 2010.
- [7] M. Modsching, R. Kramer, and K. Ten Hagen, "Field trial on GPS accuracy in a medium size city: The influence of built-up," in *Proc. 3rd Workshop Positioning, Navigat. Commun.*, 2006, pp. 209–218.
- [8] D. Swaroop and J. K. Hedrick, "Constant spacing strategies for platooning in automated highway systems," *J. Dyn. Syst., Meas., Control*, vol. 121, no. 3, pp. 462–470, Sep. 1999.
- [9] Y. Morales and T. Tsubouchi, "DGPS, RTK-GPS and StarFire DGPS performance under tree shading environments," in *Proc. IEEE Int. Conf. Integr. Technol.*, Mar. 2007, pp. 519–524.
- [10] R. Parker and S. Valaee, "Vehicular node localization using received-signal-strength indicator," *IEEE Trans. Veh. Technol.*, vol. 56, no. 6, pp. 3371–3380, Nov. 2007.
- [11] T. King, H. Füller, M. Transier, and W. Effelsberg, "Dead-reckoning for position-based forwarding on highways," in *Proc. 3rd Int. Workshop Intell. Transp.*, 2006, pp. 199–204.
- [12] S. B. Cruz, T. E. Abrudan, Z. Xiao, N. Trigoni, and J. Barros, "Neighbor-aided localization in vehicular networks," *IEEE Trans. Intell. Transport. Syst.*, vol. 18, no. 10, pp. 2693–2702, Oct. 2017.
- [13] K. Lin, J. Luo, L. Hu, M. S. Hossain, and A. Ghoneim, "Localization based on social big data analysis in the vehicular networks," *IEEE Trans. Ind. Informat.*, vol. 13, no. 4, pp. 1932–1940, Aug. 2017.
- [14] F. A. Santos, A. T. Akabane, R. S. Yokoyama, A. A. F. Loureiro, and L. A. Villas, "A roadside unit-based localization scheme to improve positioning for vehicular networks," in *Proc. IEEE 84th Veh. Technol. Conf. (VTC-Fall)*, Sep. 2016, pp. 1–5.
- [15] T. Nadeem, P. Shankar, and L. Iftode, "A comparative study of data dissemination models for VANETs," in *Proc. 3rd Annu. Int. Conf. Mobile Ubiquitous Syst. - Workshops*, Jul. 2006, pp. 1–10.
- [16] T. Leinmuller, E. Schoch, and F. Kargl, "Position verification approaches for vehicular ad hoc networks," *IEEE Wireless Commun.*, vol. 13, no. 5, pp. 16–21, Oct. 2006.
- [17] A. Triwinarko, I. Dayoub, and P. Wikanta, "Using MIMO and cross layer design for VANETs: A review," in *Proc. Int. Conf. Signals Syst. (ICSigSys)*, May 2017, pp. 13–18.
- [18] D. Kosmanos, N. Prodromou, A. Argyriou, L. A. Maglaras, and H. Janicke, "MIMO techniques for jamming threat suppression in vehicular networks," *Mobile Inf. Syst.*, vol. 2016, pp. 1–9, Oct. 2016.
- [19] M. Khurana, C. Ramakrishna, and S. N. Panda, "Capacity enhancement using MU-MIMO in vehicular ad hoc network," *Int. J. Appl. Eng. Res.*, vol. 12, no. 16, pp. 5872–5883, 2017.
- [20] S. Payami and F. Tufvesson, "Channel measurements and analysis for very large array systems at 2.6 GHz," in *Proc. 6th Eur. Conf. Antennas Propag. (EUCAP)*, Mar. 2012, pp. 433–437.
- [21] M. A. M. Marinho, A. Vinel, F. Tufvesson, F. Antreich, and J. P. C. L. da Costa, "Performance assessment for distributed broadband radio localization," in *Proc. 52nd Asilomar Conf. Signals, Syst., Comput.*, Oct. 2018, pp. 20–23.
- [22] J. A. Fessler and A. O. Hero, "Space-alternating generalized expectation-maximization algorithm," *IEEE Trans. Signal Process.*, vol. 42, no. 10, pp. 2664–2677, Oct. 1994.
- [23] F. Antreich, J. A. Nassek, G. Seco-Granados, and A. L. Swindlehurst, "The extended invariance principle for signal parameter estimation in an unknown spatial field," *IEEE Trans. Signal Process.*, vol. 59, no. 7, pp. 3213–3225, Jul. 2011.
- [24] X. Yin, S. Wang, N. Zhang, and B. Ai, "Scatterer localization using large-scale antenna arrays based on a spherical wave-front parametric model," *IEEE Trans. Wireless Commun.*, vol. 16, no. 10, pp. 6543–6556, Oct. 2017.
- [25] A. Smith, *Smartphone Ownership-2013 Update*, vol. 12. Washington, DC, USA: Pew Research Center, 2013.
- [26] I. Gresham, A. Jenkins, R. Egri, C. Eswarappa, N. Kinayman, N. Jain, R. Anderson, F. Kolak, R. Wohler, S. P. Bawell, J. Bennett, and J.-P. Lanteri, "Ultra-wideband radar sensors for short-range vehicular applications," *IEEE Trans. Microw. Theory Techn.*, vol. 52, no. 9, pp. 2105–2122, Sep. 2004.
- [27] A. P. Dempster, N. M. Laird, and D. B. Rubin, "Maximum likelihood from incomplete data via the EM algorithm," *J. Roy. Stat. Soc. B.*, vol. 39, no. 1, pp. 1–22, 1977.
- [28] P. Hoehner, "A statistical discrete-time model for the WSSUS multipath channel," *IEEE Trans. Veh. Technol.*, vol. 41, no. 4, pp. 461–468, Nov. 1992.

• • •